Experimental Determination of Elastic and Rupture Properties of Printed Ninjaflex

T. Reppel and K. Weinberg

In this paper, the effect of the 3D printing procedure on the elasticity during fused deposition modeling (FDM) is investigated. The considered material with brand name Ninjaflex® is a thermoplastic polyurethane. Uniaxial tension tests are performed to identify the material properties, specifically the Young's modulus, the maximum stretch, the tensile strength and the material's fracture toughness. The influence of geometric characteristics on the material properties is studied.

From the experimental results the parameters of Ogden's hyperelastic material model are derived. A finite element simulation of the uniaxial tensile test validates the values obtained from a conditional least-square fit. In conclusion, additional to the experimentally determined rupture properties, the elastic parameters adapted to a Neo-Hookean, a Money-Rivlin and an Ogden material model of Ninjaflex are presented.

1 Introduction

Additive manufacturing, commonly known as 3D printing, has become an established method in various areas of production. It is a favorable method to produce small series or even individual parts or components. If such printed parts shall replace parts produced by traditional methods, their mechanical properties have to be comparable. Here, in particular, the influence of the printing process on the microstructure and the resulting material properties is of interest.

For applications demanding a highly elastic material, thermoplastic polyurethane (TPU) is frequently used in additive manufacturing. TPU, a subclass of thermoplastic elastomers, is usually processed in selective laser sintering or fused deposition modeling (FDM). A TPU with a wide area of applications is Ninjaflex which is provided for FDM printing in coiled filaments. During the fused deposition the basic material it is heated up to 225°C and extruded at the desired position. Ninjaflex is mainly used for seals, gaskets, plugs, leveling feet and protective applications, see Bahr et al. (2015); Yarwindran et al. (2016); Soe and Theobald (2015) for some examples.

Here we investigate this special TPU and the effect of the printing process on its material properties. We study the differences of the material parameters under quasistatic conditions when the interior geometry, i. e. the way of printing is altered. With uniaxial tension tests we identify the Young's modulus, the tensile strength, the maximum stretch as well as the toughness of the material. From the gained data we derive the parameters of Ogden's hyperelastic material model. In the sense of an inverse analysis, the determined material parameter are then compared to FE simulations of our experiments.

A short introduction to fused deposition modeling of flexible materials and it's place in the concept of additive manufacturing is presented in the next section. The whole experimental procedure is described in section 3: the preparation of the specimens, the experimental setup, the results of the uniaxial tension tests and a comparison of the material parameters. In section 4 hyperelastic material models are fitted to the obtained data and validated in FEM simulations. The paper ends with a short summary and an outlook in section 5.

2 FDM in Additive Manufacturing

The basic idea of additive manufacturing is to slice an object into a collection of layers which is then processed by the 3D printer to rebuild the object layer by layer. The decisive attribute of 3D printing is in the word *additive*, which indicates a deposition of material and is contrary to traditional manufacturing methods as milling, turning, or sawing. The latter can also be labeled as subtractive methods. In comparison to conventional printing, a 3D print is characterized by a third dimension for the resolution, the layer thickness. Depending on the printing method this quantity is in the range of $10\,\mu m$ to $300\,\mu m$, (3Dhubs, 2017). The main advantage of additive manufacturing is to generate a complex geometry quickly and with high accuracy.

In additive manufacturing three general methods are commonly used. These are selective laser sintering (SLS), fused deposition modeling (FDM) and stereolithography (SLA). While SLS and FDM are based on the processing of solid materials, SLA creates objects by hardening a liquid resin material in a light induced polymerization process. The handling of solid materials can be subdivided into extrusion (FDM) and powder bed (SLS) 3D printing. In each of these printing methods there are different subtechnologies. For example, instead of using a laser in light polymerization, one can simply use a projector and instead of SLA one would speak of digital light processing (DLP). The first FDM printer was invented in the year 1990 by Stratasys co-founder Scott Crump (Crump, 1992), even though it was not the first technology of additive manufacturing. Already in the year 1986 the SLA printing technology was registered for patent approval by Charles W. Hull (Hull, 1986). For a summary of the evolution of additive manufacturing we refer to the work of Gross et al. (2014).

The general setup of a FDM printer is shown in Fig. 1 (left). The filament is fed through a heated moving head, melt and extruded, and then deposited layer after layer in the desired shape. During the printing process at first the contour layers of the object, the so-called *shells* are printed. At next the inner region is printed in the desired geometry by filling the *infill*. Common infill shapes are rectangular, triangular, diagonal, wiggle and honeycomb. A movable platform lowers after each layer of printing to add the next layer.
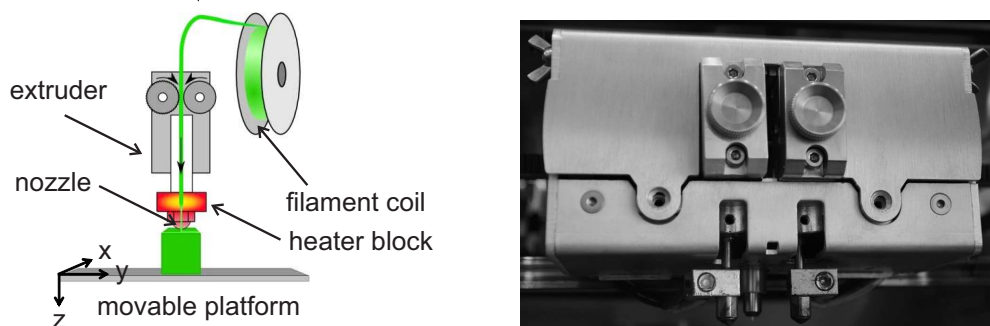

Figure 1: Principle of material deposition in FDM (left, from Clone3D (2017)) and dual extruder print head in a Leapfrog Xeed (right)

Historically the typical polymeric filament materials for FDM printers are acrylonitrile butadiene styrene (ABS) and polylactic acid (PLA). For an overview of the mechanical properties of these materials we refer to Tymrak et al. (2014). Nowadays there are plenty of other materials available including PET, Nylon and other flexible TPU formulations like Ninjaflex.

Ninjaflex manufacturer Ninjatek provides a list of material parameters based on printed specimens, see (Ninjatek, 2016). They reported results of uniaxial tensile tests which are based on ASTM D638. For specimen preparation they used a TAZ5 printer with a 0.75 mm nozzle and printed in a diagonal line fill method, the number of shell lines is not given. Ninjatek's values are presented together with our results in Table 1.
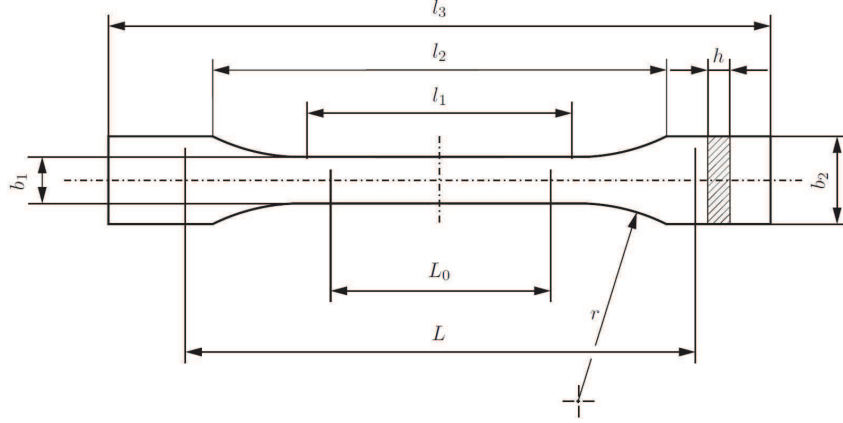
Figure 2: Specimen type 1BA from DIN EN ISO 527-2 with values: $l_3 = 75\,\text{mm}$, $l_2 = 58 \pm 2\,\text{mm}$, $l_1 = 30.0 \pm 0.5\,\text{mm}$, $L_0 = 25.0 \pm 0.5\,\text{mm}$, $L = l_2 + 2\,\text{mm}$, $h = 2\,\text{mm}$, $r = 30\,\text{mm}$, $b_2 = 10.0 \pm 0.5\,\text{mm}$ and $b_1 = 5.0 \pm 0.5\,\text{mm}$

3 Experiments

Beside the manufacturer's specifications there are hardly any reports on material properties of Ninjaflex; only some values for the elongation are presented by Tanikella et al. (2017). The few available material parameters and the lack of details of the specimens' geometry motivated us to perform experiments independently.

3.1 Specimen Preparation

The specimens for the uniaxial tensile test were printed with a Leapfrog Xeed FDM printer with a nozzle diameter of $0.35\,\text{mm}$, see Fig. 1 (right). One extruder is used; the positioning in x and y-direction is carried out by the print head, the platform is movable in z-direction. The geometry was chosen according to DIN EN ISO 527-2 type 1BA, see Fig. 2, with a thickness of $t = 2\,\text{mm}$. The layer height in z-direction was set to $0.286\,\text{mm}$ for each of the seven layers. Each layer's shell was filled in a diagonal $45°$ pattern, see Fig. 3 (middle and right). Note that after each layer the diagonal pattern was mirrored to reduce the influence of the infill geometry on macroscopic properties.

With the aim to investigate the differences of the mechanical properties, the specimens were printed with the minimum and maximum shell width. The obvious minimum was one outside line (specimen of type 005) and the possible maximum was a shell consisting of four lines (specimen of type 002), see Fig. 3. For both types we printed and tested six specimens each.

3.2 Uniaxial Tension Tests

A Hegewald & Peschke Inspekt 100 testing machine was used for our experiments. The specimens were fixed with hydraulic clamps at 120 bar. The 25 kN load cell is suitable being a class 1 load cell according
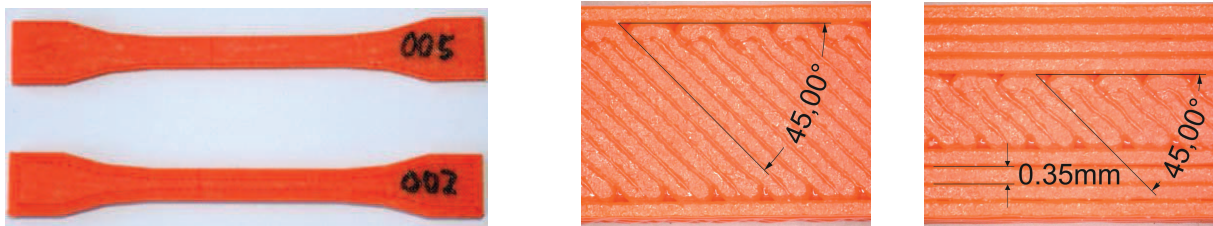

Figure 3: Specimens printed according to DIN EN ISO 527-2 with 58 mm distance between shoulders (left). Closeup of specimen type 005 (middle) with one and type 002 (right) with four shell lines
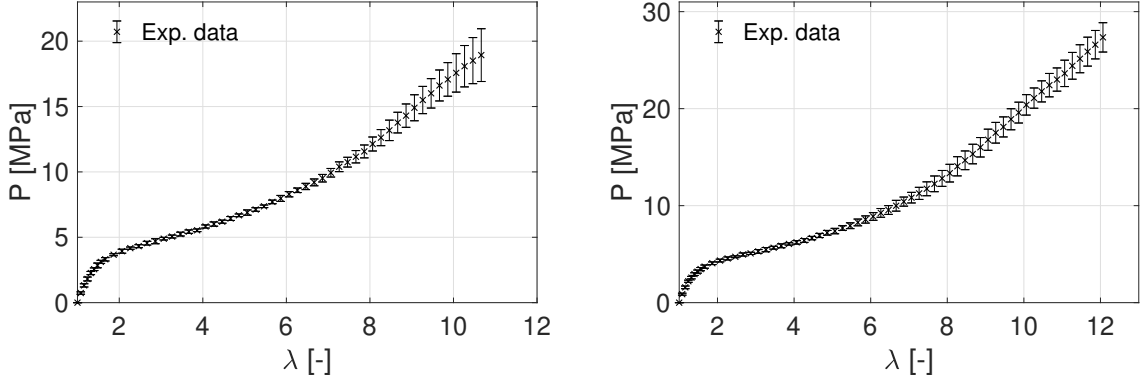
Figure 4: Nominal stress P [MPa] with a 95% confidence interval over stretch λ [-] for specimen of type 005 (left) and specimen of type 002 (right)

to DIN EN ISO 7500-1. The whole experimental procedure was performed following DIN EN ISO 527-1, i.e. applying tension until failure with $1\,\mathrm{mm/s}$. The time, the applied displacement and the measured force were recorded with $50\,\mathrm{Hz}$.

The displacement and the measured force determine the engineering strain $\epsilon = \Delta L/L_0$ and the nominal stress $P = F/(b_1 t)$. Then the stretch $\lambda = 1 + \epsilon$ and the average nominal stress P [MPa] were calculated with a 95% confidence interval. The Young's modulus E is given by the slope in the linear range of the stress-strain-curve and from the total stress-strain-curve we calculate the material's toughness as the work of fracture (ASTM D638; Heyden et al., 2014),

$$W = \int_0^{\epsilon_\mathrm{max}} P \, \mathrm{d}\epsilon \,. \tag{1}$$

The stress-strain curves are shown in Fig. 4; all results are summarized in Table 1.

Both types of specimen reached an elongation of more than 1100% with a maximum tensile strength of $19.2\,\mathrm{MPa}$ (type 005) and $27.8\,\mathrm{MPa}$ (type 002). At an elongation of 800% we measured an average nominal stress of $11.96 \pm 0.57\,\mathrm{MPa}$ for type 005 which is comparable to the value reported by Tanikella et al. (2017). The calculated Young's modulus E is clearly higher for the specimen of type 002. This is likely due to a higher proportion of the shell which is oriented in the direction of tension and seems to stiffen the specimens. Both values for E are also in good agreement with the manufacturer's value. This is contrary to the maximum stretch where our specimens (type 002) reached about twice as much of elongation. With a similar maximum stress of $27.8\,\mathrm{MPa}$ the resulting material toughness is also higher in our experiments.

Property	Specimen 005	Specimen 002	Manufacturer
Elongation [%]	1139±42	1200±36	660
Tensile strength [MPa]	19.2±1.98	27.8±1.63	26
Young's modulus [MPa]	10.7±0.38	12.2±0.13	12
Toughness [$\cdot 10^6$ J / m^3]	88.7±4.45	133.4±7.03	82.7

Table 1: Ninjaflex material properties obtained in our tensile tests and provided by the manufacturer

3.3 Rupture Behavior

A direct comparison of the stress-strain curves for both specimen groups is given in Fig. 5 (left) and shows that the printing procedure has a significant effect for large strains only. A thicker shell results in a higher resistance of the specimens at more than 600% stretch. Also the maximum stretch at rupture is about 53% higher for specimen of type 002. Generally specimens of type 005 showed a proper behavior in terms of a homogeneous tensile specimen, Fig. 5 (middle). The failure happened always in the designated area in the middle of the specimen. As can be seen in the photograph, the specimen showed a bit of

delamination which is a result of material anisotropy inside the specimen. At the same time, this group of specimens showed a higher deviation in the stress-strain curves starting at about 800% stretch.

Specimens of type 005 have to be regarded more critically. In Fig. 5 (right) we see that the four-line shell has a massive effect on the failure mechanism. In most of the cases, the shell separated from the infill in a delamination process near to the point, where the specimen was clamped. This points on a lack of adhesion between shell and infill. In some cases the diagonal infill even ruptured while the shell was still intact. In the displayed stress-strain curve we plot only the values before such separation and rupture arise. Therefore, on the one hand, the validity of the uniaxial tensile test with specimen of type 002 is limited at very high stretches. On the other hand, the deviation of the nominal stress is lower in stretches up to 700%.
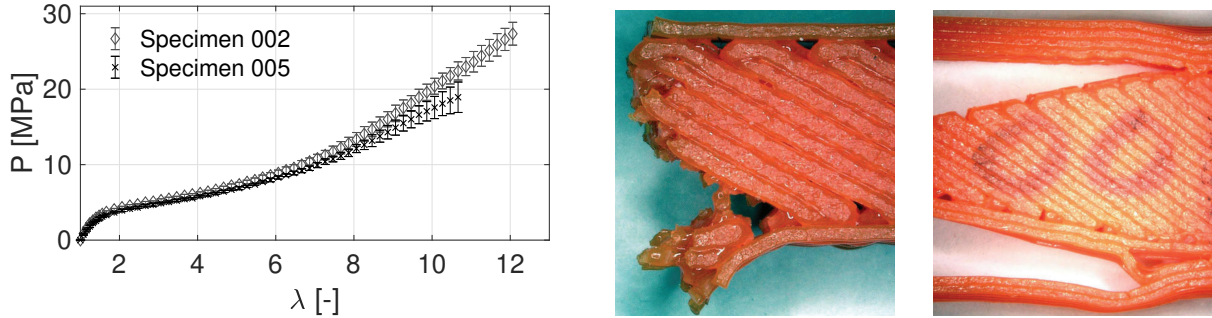

Figure 5: Comparison of average nominal stress over stretch (left); closeup of a ruptured specimen of type 005 (middle) and of type 002 (right)

4   Hyperelastic Modeling

Although the tensile test specimens show a certain directional dependence due to the printing process, the material is not anisotropic in the classical sense, i.e., there are neither differing degrees of stiffness nor supporting fibers. Therefore we presume a homogenous isotropic behavior, an approach which was also chosen by Berselli et al. (2011) for hyperelastic and by many others for linear-elastic structures in additive manufacturing.

The TPU material Ninjaflex belongs to the class of incompressible hyperelastic materials. Since the classic Neo-Hookean formulation of Treloar (1944), many different approaches have been developed here; for an comprehensive overview we refer to Reppel et al. (2013), Hoss and Marczak (2010) and Marckmann and Verron (2006).

The fundamental relation of all elastic models is the strain energy density Ψ which will here be stated as a function of the principal stretches λ_a, $a = 1, 2, 3$. The principal components of the first Piola-Kirchhoff stresses follow as $P_a = \partial\Psi/\partial\lambda_a$ and for isotropic incompressible material it can be specified to

$$P_a(\lambda) = -\frac{1}{\lambda_a}p + \frac{\partial\Psi}{\partial\lambda_a} \tag{2}$$

with p to be determined from uniaxial tension with $P_1 = P$ and $P_2 = P_3 = 0$, cf. Holzapfel (2000).

For a strain energy density which is expressed in terms of the first and second invariant of deformation, I_1 and I_2, the principal first Piola-Kirchhoff stress can directly be evaluated to

$$P(\lambda) = 2\left(\lambda - \frac{1}{\lambda^2}\right)\frac{\partial\Psi}{\partial I_1} + 2\left(1 - \frac{1}{\lambda^3}\right)\frac{\partial\Psi}{\partial I_2}. \tag{3}$$

The fundamental hyperelastic material models have a strain energy of the form

$$\Psi(I_1, I_2) = \frac{\mu_1}{2}(I_1 - 3) + \frac{\mu_2}{2}(I_2 - 3) \tag{4}$$

which corresponds to the Mooney-Rivlin model for $\mu_1 + \mu_2 = \mu$ and to the Neo-Hookean model for $\mu_1 = \mu$, $\mu_2 = 0$. Here and below μ is the initial shear modulus. The principal first Piola-Kirchhoff stress follows
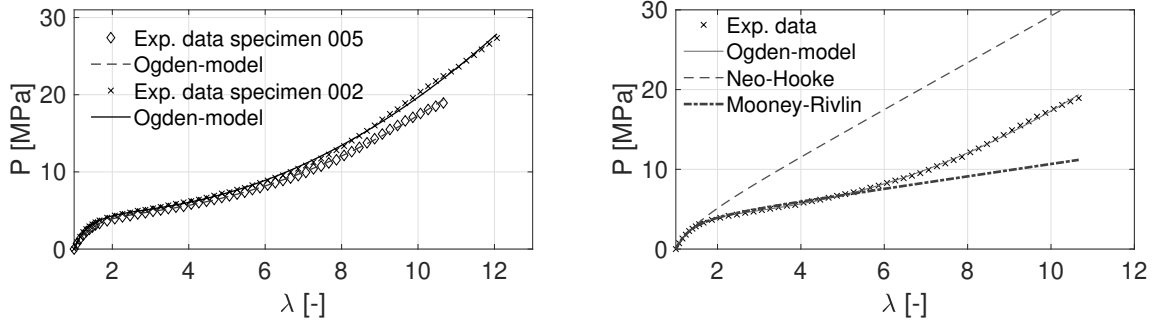
Figure 6: Experimental data and fitted Ogden model for both specimen types (left). Experimental data of type 005 and fit of different hyperleastic models (right).

from (3) as

$$P(\lambda) = \mu_1 \left(\lambda - \frac{1}{\lambda^2} \right) + \mu_2 \left(1 - \frac{1}{\lambda^3} \right) . \tag{5}$$

Both models are simple and convenient and can be used to describe the elastic behaviour of Ninjaflex for elastic elongation up to 200-600%. To address the very high elongation of more than $1200\,\%$ in our experiments, a more elaborate hyperelastic model is required. The general Ogden model for incompressible elastic material (Ogden, 1972) expresses the strain energy density as

$$\Psi(\lambda_1, \lambda_2, \lambda_3) = \sum_{p=1}^{N} \frac{\mu_p}{\alpha_p} \left(\lambda_1^{\alpha_p} + \lambda_2^{\alpha_p} + \lambda_3^{\alpha_p} - 3 \right) \quad \text{with} \quad \sum_{p=1}^{N} \mu_p \alpha_p = 2\mu \, , \tag{6}$$

where N and μ_p, α_p are material constants. From (2) and (6) we derive the first Piola-stress in uniaxial tension to have the form

$$P(\lambda) = \sum_{p=1}^{N} \mu_p \left(\lambda^{\alpha_p - 1} - \lambda^{-\alpha_p/2 - 1} \right) . \tag{7}$$

In the next step a conditional nonlinear least-square method is used to fit Eq. (7) to our measured data. The constraint is Hill's criterion (Hill, 1970)

$$\mu_p \alpha_p > 0 \, , \forall p = 1, \ldots, N \, , \tag{8}$$

which ensures material stability. This constraint is applied to a conditional nonlinear least-square fit using Matlab's `fmincon` algorithm with maximum 10^9 iterations and the interior-point method. We start with $N = 1$ parameter pair and the constraints $\mu_1 > 0$, $\alpha_1 > 0$. In the next step, this is compared to the result with the constraints $\mu_1 < 0$, $\alpha_1 < 0$. The quality of the fit is measured by the coefficient of determination R^2. We now increase N and calculate all possible combinations of the algebraic sign ($\pm$) of μ_p and α_p with $\mu_p \alpha_p > 0$. Ogden's model is fitted with all parameter sign combinations to our data points. If the maximum of R^2 of those fits is smaller or equal than the R^2 of $N - 1$ parameters, we stop and chose $N - 1$ parameters. In the other case we increase N again.

p	μ_p [MPa]	α_p [-]	p	μ_p [MPa]	α_p [-]
1	0.13	3.05	1	1.13	3.11
2	-1214	-0.0054	2	-13.17	-0.60

μ [MPa]	R^2 [-]	μ [MPa]	R^2 [-]
3.58	99.94%	4.14	99.92%

Table 2: Ogden model material parameters for $N = 2$, resulting shear modulus μ and coefficient of determination R^2 for the specimen of type 005 (left) and for the specimen of type 002 (right)

It turns out, that there is no improvement of the accuracy for $N > 2$, so with only four parameters, the pure hyperelastic behavior of the material is described. The result is shown in Fig. 6, the resulting parameters are listed in Table 2.

Also in Fig. 6 the parameter fits for the Neo-Hookean model and the Mooney-Rivlin model to the experimental data of the specimen with one-line shell are displayed. We see clearly, that a Neo-Hookean is not able to match the stress-strain curve for for a significant amount of straining. Up to $\epsilon \leq 70\%$ the Neo-Hookean model is sufficient with a coefficient of determination of $R^2 = 0.99$. The two-parameter fit of the Mooney-Rivlin model allows with an analog strategy for 450% of straining ($R^2 = 0.97$). Please note that here the initial shear modulus is higher which basically follows from a relatively large value of μ_2 which, however, has to be considered carefully. The two Mooney-Rivlin parameters, specifically the second term in (5), cannot uniquely be identified in uniaxial tension. The situation is similar for the Ogden parameters; to obtain generally valid parameter sets additional experiments, e.g. biaxial tests, are necessary.

	μ_1 [MPa]	μ_2 [MPa]	μ [MPa]
Neo-Hooke	-	-	2.93
Mooney-Rivlin	0.77	2.94	3.72

Table 3: Material parameters of the Neo-Hookean and the Mooney-Rivlin model

To validate the parameters gained from the conditional least-square fit, we apply the results to an Abaqus simulation of the tensile test. The usage of hybrid hexahedral elements (C3D8H) provides a stable incompressible hyperelastic simulation. Since the Odgen model is implemented in Abaqus in the Valanis and Landel (1967) formulation, the parameters μ_p are converted to:

$$\tilde{\mu}_p = \frac{\mu_p \alpha_p}{2} \tag{9}$$

The true stress is evaluated in one point in the center of the model, whereby the true stress is transformed back to the nominal, i.e. the first Piola-Kirchhoff stress. The results are displayed in Fig. 7 and show agreement to the experimental results.
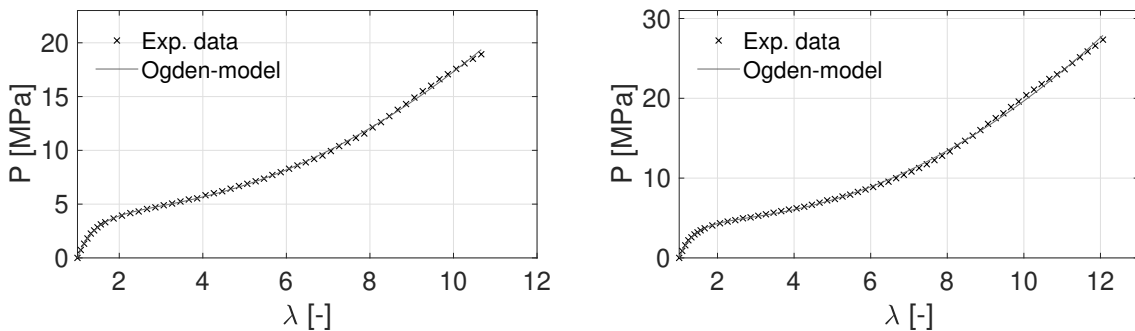

Figure 7: Nominal stress over stretch; experimental data and Abaqus simulation with C3D8H elements for specimen of type 005 (left) and specimen of type 002 (right)

5 Summary and Outlook

In this contribution we presented the results of our uniaxial tensile tests of FDM printed specimens consisting of a proprietary TPU material called Ninjaflex. To show the effect of the interior geometry two sets of specimen, one with one-line shell which is the minimum and one with the upper limit of four shell lines, are printed.

Ninjaflex is highly elastic and up to 600% of elongation the material response is basically the same for both types of specimen. The measured elastic parameters are in the expected range and confirmed by some data provided by the manufacturer. The differences in the failure stretch and material toughness

can be explained by the unknown printing pattern inside of the manufacturer's specimen. Also the standardized experiments (DIN and ASTM) differ slightly in terms of the specimen's geometry and the test speed. The elastic modulus and the obtain parameters for rupture are given in Table 1.

Still being non-isotropic materials the specimen with one-line shell showed an almost homogeneous material behavior, i.e. straight rupture in the middle of the specimen. At the same time the deviation of the measured stresses was relatively high. The specimen with four-line shells showed a stiffer response, a lower stress deviation but an improper failure behavior. Due to a loss of adhesion the infill delaminates from the shell in the zone of the fixture, i.e. where the specimen was clamped. This results in a failure of the infill with the shell layers still being unimpaired. For future works we therefore suggest to print tensile specimens with a one-line shell only to ensure a homogeneous material behavior.

To find the optimal number and values of the parameters in Ogden's material model, we applied an algorithm based on the conditional nonlinear least-square method. It came out that only two pairs of parameters are needed to render the measured experimental data in a proper way. The obtained values are implemented in an Abaqus simulation of the uniaxial tensile test using hybrid elements to account for the incompressible material behavior. The results are consistent with the experimental data and replicate the stress-strain curves.

In uniaxial tension we identified the following material parameters for the Ogden model: $\mu_1 = 0.133\,\mathrm{MPa}$, $\alpha_1 = 3.05$, $\mu_2 = -1214\,\mathrm{MPa}$, $\alpha_2 = -0.0054$. This results in a shear modulus of $\mu = 3.58\,\mathrm{MPa}$ and a Young's modulus of $E = 12.42\,\mathrm{MPa}$. For the Neo-Hookean model, which is only valid for a strain of less than 70%, we suggest to use a shear modulus of $\mu = 2.93\,\mathrm{MPa}$. For the Mooney-Rivlin model, which is valid for a strain up to 450%, we propose values of $\mu_1 = 0.77\,\mathrm{MPa}$ and $\mu_2 = 2.94\,\mathrm{MPa}$. All values are also summarized in Table 3.

In future we plan additional experiments to validate the elastic and to study the viscoelastic material behavior of Ninjaflex. Specifically, we will investigate the dynamic properties of flexible materials by Split-Hopkinson-Pressure Bar experiments of printed cylindrical specimens.

References

3Dhubs: The impact of layer height on a 3d print. `https://www.3dhubs.com/knowledge-base/impact-layer-height-3d-print` (2017), [Online; accessed 19-July-2017].

ASTM D638: Standard test method for tensile properties of plastics (2003).

Bahr, R.; Le, T.; Tentzeris, M. M.; Moscato, S.; Pasian, M.; Bozzi, M.; Perregrini, L.: RF characterization of 3d printed flexible materials-ninjaflex filaments. In: *Microwave Conference (EuMC), 2015 European*, pages 742–745, IEEE (2015).

Berselli, G.; Vertechy, R.; Pellicciari, M.; Vassura, G.: Hyperelastic modeling of rubber-like photopolymers for additive manufacturing processes. In: *Rapid Prototyping Technology-Principles and Functional Requirements*, InTech (2011).

Clone3D: FDM, fused deposition modelling. `http://www.clone3d.co.nz/printer-and-plastic/` (2017), [Online; accessed 19-July-2017].

Crump, S.: Apparatus and method for creating three-dimensional objects (Jun. 9 1992), U.S. Patent 5,121,329.

DIN EN ISO 527-1: Kunststoffe – Bestimmung der Zugeigenschaften – Teil 1: Allgemeine Grundsätze (Jun. 2012).

DIN EN ISO 527-2: Kunststoffe – Bestimmung der Zugeigenschaften – Teil 2: Prüfbedingungen für Form– und Extrusionsmassen (Jun. 2012).

DIN EN ISO 7500-1: Metallische Werkstoffe – Kalibrierung und Überprüfung von statischen einachsigen Prüfmaschinen – Teil 1: Zug– und Druckprüfmaschinen – Kalibrierung und Überprüfung der Kraftmesseinrichtung (May 2016).

Gross, B. C.; Erkal, J. L.; Lockwood, S. Y.; Chen, C.; Spence, D. M.: Evaluation of 3d printing and its potential impact on biotechnology and the chemical sciences. *Analytical Chemistry*, 86, 7, (2014), 3240–3253.

Heyden, S.; Li, B.; Weinberg, K.; Conti, S.; Ortiz, M.: A micromechanical damage and fracture model for polymers based on fractional strain-gradient elasticity. *Journal of the Mechanics and Physics of Solids*, DOI: 10.1016/j.jmps.2014.08.005.

Hill, R.: Constitutive inequalities for isotropic elastic solids under finite strain. In: *Proceedings of the Royal Society of London A: Mathematical, Physical and Engineering Sciences*, vol. 314, pages 457–472, The Royal Society (1970).

Holzapfel, A. G.: *Nonlinear Solid Mechanics II*. John Wiley & Sons, Inc. (2000).

Hoss, L.; Marczak, R.: A new constitutive model for rubber-like materials. *Mecanica Computacional*, 29, (2010), 2759–2773.

Hull, C.: Apparatus for production of three-dimensional objects by stereolithography (Mar. 11 1986), U.S. Patent 4,575,330.

Marckmann, G.; Verron, E.: Comparison of hyperelastic models for rubber-like materials. *Rubber chemistry and technology*, 79, 5, (2006), 835–858.

Ninjatek: Technical specifications of NinjaFlex. `https://ninjatek.com/wp-content/uploads/2016/05/NinjaFlex-TDS.pdf` (2016), [Online; accessed 19-July-2017].

Ogden, R.: Large deformation isotropic elasticity – on the correlation of theory and experiment for incompressible rubberlike solids. *Proceedings of the Royal Society of London. A. Mathematical and Physical Sciences*, 326, 1567, (1972), 565–584.

Reppel, T.; Dally, T.; Weinberg, K.: On the elastic modeling of highly extensible polyurea. *Technische Mechanik*, 33, 1, (2013), 19–33.

Soe, S.; Theobald, P.: Energy absorbing characteristics of additively manufactured tpe cellular structures. In: *2nd International Conference on Sustainable Design and Manufacturing* (2015).

Tanikella, N. G.; Wittbrodt, B.; Pearce, J. M.: Tensile strength of commercial polymer materials for fused filament fabrication 3d printing. *Additive Manufacturing*, 15, (2017), 40–47.

Treloar, L. R. G.: Stress-strain data for vulcanized rubber under various types of deformation. *Proceedings of the Faraday Society*, 40, (1944), 59–70.

Tymrak, B.; Kreiger, M.; Pearce, J. M.: Mechanical properties of components fabricated with open-source 3-d printers under realistic environmental conditions. *Materials & Design*, 58, (2014), 242–246.

Valanis, K.; Landel, R. F.: The strain-energy function of a hyperelastic material in terms of the extension ratios. *Journal of Applied Physics*, 38, 7, (1967), 2997–3002.

Yarwindran, M.; Azwani Sa'aban, N.; Ibrahim, M.; Periyasamy, R.: Thermoplastic elastomer infill pattern impact on mechanical properties 3d printed customized orthotic insole. *ARPN Journal of Engineering and Applied Sciences*, 11, 10, (2016), 6519–6524.

Address: Universität Siegen, Fakultät IV, Dept. Maschinenbau, Lehrstuhl für Festkörpermechanik, Paul-Bonatz-Str. 9-11, D-57076 Siegen, Germany
email: `thomas.reppel | kerstin.weinberg@uni-siegen.de`